Nonequilibrium magnetic properties in a two-dimensional kinetic mixed Ising system within the effective-field theory and Glauber-type stochastic dynamics approach

Mehmet Ertaş,[1] Bayram Deviren,[2] and Mustafa Keskin[1,*]
[1]*Department of Physics, Erciyes University, 38039 Kayseri, Turkey*
[2]*Department of Physics, Nevsehir University, 50300 Nevşehir, Turkey*
(Received 9 July 2012; published 7 November 2012)

Nonequilibrium magnetic properties in a two-dimensional kinetic mixed spin-2 and spin-5/2 Ising system in the presence of a time-varying (sinusoidal) magnetic field are studied within the effective-field theory (EFT) with correlations. The time evolution of the system is described by using Glauber-type stochastic dynamics. The dynamic EFT equations are derived by employing the Glauber transition rates for two interpenetrating square lattices. We investigate the time dependence of the magnetizations for different interaction parameter values in order to find the phases in the system. We also study the thermal behavior of the dynamic magnetizations, the hysteresis loop area, and dynamic correlation. The dynamic phase diagrams are presented in the reduced magnetic field amplitude and reduced temperature plane and we observe that the system exhibits dynamic tricritical and reentrant behaviors. Moreover, the system also displays a double critical end point (B), a zero-temperature critical point (Z), a critical end point (E), and a triple point (TP). We also performed a comparison with the mean-field prediction in order to point out the effects of correlations and found that some of the dynamic first-order phase lines, which are artifacts of the mean-field approach, disappeared.

DOI: 10.1103/PhysRevE.86.051110 PACS number(s): 05.50.+q, 05.70.Fh, 64.60.Ht, 75.10.Hk

I. INTRODUCTION

At present, the equilibrium behavior of cooperative physical systems is rather well known within the framework of equilibrium statistical physics [1]. On the other hand, the dynamic properties of the systems are not yet well known, either theoretically or experimentally, due to their complexity. Some interesting problems in dynamic systems are the dynamic phase transition (DPT) or the nonequilibrium phase transition, in which the mechanism behind it has not yet been explored rigorously and the basic phenomenology is still undeveloped. Hence, further efforts to solve these challenging time-dependent problems, especially calculating the DPT points and constructing the phase diagram, should be rewarding. The DPT in a nonequilibrium system in the presence of an oscillating external magnetic field has attracted much attention in recent years, theoretically (see [2–8] and references therein). Experimental evidence for the DPT has been found in highly anisotropic (Ising-like) and ultrathin Co/Cu(001) ferromagnetic films [9], amorphous YBaCuO films [10], in ferroic systems (ferromagnets, ferroelectrics, and ferroelastics) with pinned domain walls [11], ultrathin magnetic $[Co(0.4nm)/Pt(0.7nm)]_3$ multilayers [12], polyethylene naphthalate (PEN) nanocomposites [13], and cuprates [14].

On the other hand, during the past few decades, both experimental and theoretical efforts towards an understanding of the magnetic properties of mixed spin Ising systems have been made. One of the main reasons for the increasing interest in these systems is related to their possible useful properties for technological applications in thermomagnetic recording [15]. Since mixed spin Ising systems have less translational symmetry than their single spin counterparts, they also exhibit many new phenomena which cannot be observed in single spin Ising systems, and the study of these systems may be important for an understanding of bimetallic molecular-systems-based magnetic materials that have properties such as low density, electrical insulation, and low-temperature fabrication [16]. Moreover, these systems are well adapted to study a certain type of ferrimagnetism and are of great interest because of their interesting and possible useful properties for technological applications as well as academic research. One of the well known and most studied mixed spin Ising systems is the mixed spin-2 and spin-5/2 Ising system. This system provides good models to investigate ferrimagnetic materials that are currently the subject of a great deal of interest due to their possible useful properties for technological applications as well as academic research. The mixed spin (2, 5/2) Ising system is also the prototypical system that has been used for studying the magnetic behaviors of molecular-based magnetic materials such as $A\mathrm{Fe^{II}Fe^{III}}(\mathrm{C_2O_4})_3$ [$A = \mathrm{N}(n\text{-}\mathrm{C}_n\mathrm{H}_{2n+1})_4$, $n = 3$–5] [17–23]. The exact solution of the mixed spin (2, 5/2) Ising system was also studied on the Bethe lattice by means of exact recursion relations [24].

While the equilibrium properties of the mixed spin-2 and spin-5/2 Ising system have been investigated in detail, the nonequilibrium properties of the system have not been as thoroughly explored. An early attempt to study the magnetic properties of a nonequilibrium mixed spin (2, 5/2) Ising ferrimagnetic system on a hexagonal lattice was made by Keskin and Ertaş [3]. They studied the existence of dynamic compensation temperatures and also presented the dynamic phase diagram within the mean-field approach and Glauber-type stochastic dynamics. Bukharov *et al.* [25] analyzed a magnetic dynamic hysteresis of Co-based quasi-1D ferrimagnets within the model of the mixed spin-2 and spin-5/2 Ising chain by using Glauber-type stochastic dynamics. Recently, Ertaş *et al.* [26] studied multicritical dynamic phase diagrams and dynamic hysteresis loops, within a mean-field approach, in the mixed spin-2 and spin-5/2 Ising ferrimagnetic system with repulsive biquadratic coupling in the presence of a time-varying (sinusoidal) magnetic field by employing Glauber-type

*Corresponding author: keskin@erciyes.edu.tr

stochastic dynamics. Moreover, Ertaş *et al.* [27] also investigated the dynamic magnetic properties, in particular, the behavior of dynamic magnetic hysteresis, in the kinetic mixed spin (2, 5/2) Ising model on a layered honeycomb lattice that corresponds to the molecular-based magnetic materials $A\mathrm{Fe^{II}Fe^{III}}(\mathrm{C_2O_4})_3$ [$A = \mathrm{N}(n\text{-}\mathrm{C}_n\mathrm{H}_{2n+1})_4$, $n = 3$–5] in which $\mathrm{Fe^{II}}$ ($S = 5/2$) and $\mathrm{Fe^{III}}$ ($\sigma = 2$) occupy sites.

The purpose of the present paper is to study the dynamic magnetic properties of a two-dimensional kinetic mixed spin-2 and spin-5/2 Ising system in the presence of a time-varying (sinusoidal) magnetic field within the effective-field theory (EFT) with correlations and using Glauber-type stochastic dynamics. The dynamic EFT equations are derived by employing the Glauber transition rates for two interpenetrating square lattices. In particular, we investigated the time dependence of the magnetizations for different interaction parameter values in order to find the phases in the system. Then, the thermal behavior of the dynamic magnetizations, the hysteresis loop area, and the dynamic correlation were investigated, and the dynamic phase diagrams were presented in the reduced-temperature and magnetic field amplitude plane. We also performed a comparison with the mean-field prediction in order to point out the effects of correlations and found that some of the dynamic first-order phase lines, which are artifacts of the mean-field approach, disappeared. We should also mention that the EFT method can incorporate some effects of spin-spin correlations, without introducing mathematical complexity, by using the Van der Waerden identities and can provide results that are quite superior to those obtained by using the mean-field approximation (MFA). Therefore, recently, the EFT was generalized to study the DPT in the kinetic spin-1/2 [4–6] and spin-1 [7] Ising systems in the presence of a sinusoidal oscillating external magnetic field. To the best of our knowledge, this work is an early attempt to study the DPT in the kinetic mixed Ising system in the presence of a time-varying (sinusoidal) magnetic field within the framework of the EFT with correlations and using Glauber-type stochastic dynamics.

The outline of the remaining part of this paper is organized as follows. In Sec. II, the model and its formulations, namely, the derivation of the set of dynamic equations, are briefly given. In Sec. III, the results of the time variations in average magnetizations and the thermal behaviors of the dynamic magnetizations, the hysteresis loop area, and the dynamic correlation are presented. The dynamic phase diagrams are also discussed and compared with the dynamic mean-field results. Finally, the summary and conclusion are given in Sec. IV.

II. MODEL AND FORMULATIONS

A. Model

The mixed spin-2 and spin-5/2 Ising model is described as a two-sublattice system, with spin variables $\sigma_i = \pm 2, \pm 1, 0$ and $S_j = \pm 5/2, \pm 3/2, \pm 1/2$ on the sites of sublattices A and B, respectively. In the underlying lattice the sites of sublattice A are occupied by spins σ_i, while those of sublattice B are occupied by spins S_j. The Hamiltonian of the system is given by

$$H = -J \sum_{\langle ij \rangle} \sigma_i S_j - D \left[\sum_i \sigma_i^2 + \sum_j S_j^2 \right] - h(t) \left[\sum_i \sigma_i + \sum_j S_j \right], \tag{1}$$

where $\langle ij \rangle$ indicates a summation over all pairs of nearest-neighboring sites, J is the bilinear nearest-neighbor exchange interaction, D is the crystal-field interaction or single-ion anisotropy, and $h(t)$ is a time-dependent external oscillating magnetic field and is given by

$$h(t) = h_0 \sin(wt), \tag{2}$$

where h_0 and $w = 2\pi\nu$ are the amplitude and the angular frequency of the oscillating field, respectively. The system is in contact with an isothermal heat bath at absolute temperature T_A.

B. Derivation of dynamic effective-field equations

We apply the Glauber-type stochastic dynamics [28], in particular, we employ Glauber transition rates, to obtain the set of dynamic effective-field equations. Thus, the system evolves according to a Glauber-type stochastic process at a rate of $1/\tau$ transitions per unit time; hence the frequency of spin flipping, f, is $1/\tau$. Leaving the S spins fixed, we define $P^A(\sigma_1,\sigma_2,\ldots,\sigma_N;t)$ as the probability that the system has the σ-spin configuration$\sigma_1, \sigma_2, \ldots, \sigma_N; t$, at time t. Also, by leaving the σ spins fixed, we define $P^B(S_1,S_2,\ldots,S_N;t)$ as the probability that the system has the S-spin configuration, $S_1,S_2,\ldots,S_N$ at time t. Then, we calculate $W_i^A(\sigma_i \to \sigma_i')$ and $W_j^B(S_j \to S_j')$, the probabilities per unit time that the ith σ spin changes from σ_i to σ_i' (while the S spins are momentarily fixed) and the jth S spin changes from S_j to S_j' (while the σ spins are momentarily fixed), respectively. Thus, if the S spins on the layers B are momentarily fixed, the master equation for the σ spins on layers A can be written as

$$\begin{aligned}\frac{d}{dt}P^A(\sigma_1,\sigma_2,\ldots,\sigma_N;t) = &-\sum_i \left(\sum_{\sigma_i \neq \sigma_i'} W_i^A(\sigma_i \to \sigma_i') \right) \\ &\times P^A(\sigma_1,\sigma_2,\ldots,\sigma_i,\ldots,\sigma_N;t) \\ &+ \sum_i \left(\sum_{\sigma_i \sigma_i'} W_i^A(\sigma_i' \to \sigma_i) \right) \\ &\times P^A(\sigma_1,\sigma_2,\ldots,\sigma_i',\ldots,\sigma_N;t),\end{aligned} \tag{3}$$

where $W_i^A(\sigma_i \to \sigma_i')$ is the probability per unit time that the ith spin changes from the value σ_i to σ_i'. Since the system is in contact with a heat bath at absolute temperature T_A, each spin can change from the value σ_i to σ_i', with the probability per unit time

$$W_i^A(\sigma_i \to \sigma_i') = \frac{1}{\tau} \frac{\exp[-\beta\, \Delta E^A(\sigma_i \to \sigma_i')]}{\sum_{\sigma_i'} \exp[-\beta\, \Delta E^A(\sigma_i \to \sigma_i')]}, \tag{4}$$

where $\beta = 1/k_B T_A$, k_B is the Boltzmann factor, $\sum_{\sigma_i'}$ is the sum over the five possible values of $\sigma_i' = \pm 2, \pm 1, 0$, and

$$\Delta E^A(\sigma_i \to \sigma_i') = -(\sigma_i \to \sigma_i')\left(J\sum_j S_j^B + h(t)\right) - [(\sigma_i')^2 - (\sigma_i)^2]D \tag{5}$$

gives the change in the system's energy when the σ_i spin changes. The probabilities satisfy the detailed balance condition

$$\frac{W_i^A(\sigma_i \to \sigma_i')}{W_i^A(\sigma_i' \to \sigma_i)} = \frac{P^A(\sigma_1, \sigma_2, \ldots, \sigma_i', \ldots, \sigma_N)}{P^A(\sigma_1, \sigma_2, \ldots, \sigma_i, \ldots, \sigma_N)}, \tag{6}$$

and the probabilities $W_i^A(\sigma_i \to \sigma_i')$ are given in Appendix A. From the master equation associated with the stochastic process, it follows that the average $\langle \sigma_i^A \rangle$ satisfies the following equation:

$$\tau \frac{d}{dt}\langle \sigma_i^A \rangle = -\langle \sigma_i^A \rangle + \left\langle \frac{2\exp(4\beta D)\,\sinh(2\beta[E_i + h(t)]) + \exp(\beta D)\sinh(\beta[E_i + h(t)])}{\exp(4\beta D)\,\cosh(2\beta[E_i + h(t)]) + \exp(\beta D)\cosh(\beta[E_i + h(t)]) + 1/2} \right\rangle, \tag{7}$$

where $\langle \ldots \rangle$denotes the canonical thermal average and $E_i = J\sum_j S_j^B$. Now, assuming that the σ spins on layers A are momentarily fixed and that the S spins on layers B change, we can obtain the second dynamic equation for the S spins on layers B by using similar calculations as

$$\tau \frac{d}{dt}\langle S_j^B \rangle = -\langle S_j^B \rangle + \left\langle \frac{5\sinh\left(\frac{5\beta}{2}[E_j + h(t)]\right) + 3\exp(-4\beta D)\,\sinh\left(\frac{3\beta}{2}[E_j + h(t)]\right) + \exp(-6\beta D)\sinh\left(\frac{\beta}{2}[E_j + h(t)]\right)}{2\cosh\left(\frac{5\beta}{2}[E_j + h(t)]\right) + 2\exp(-4\beta D)\cosh\left(\frac{3\beta}{2}[E_j + h(t)]\right) + 2\exp(-6\beta D)\cosh\left(\frac{\beta}{2}[E_j + h(t)]\right)} \right\rangle, \tag{8}$$

where $E_j = J\sum_i \sigma_i^A$.

We now use the EFT with correlations to obtain the set of dynamic effective-field equations. This method was first introduced by Honmura and Kaneyoshi [29] and Kaneyoshi *et al.* [30], where a more advanced method is used in dealing with Ising systems than the mean field theory (MFT), because it considers more correlations. The main problem is to evaluate the thermal average of the last terms in Eqs. (7) and (8). The starting point to determine the statistics of the present spin system is the exact relation due to Callen [31]. The EFT with correlations is also convenient to introduce the differential operator technique into expressions of the last terms in Eqs. (7) and (8),

$$\left\langle \frac{2\exp(4\beta D)\,\sinh(2\beta[E_i + h(t)]) + \exp(\beta D)\sinh(\beta[E_i + h(t)])}{\exp(4\beta D)\,\cosh(2\beta[E_i + h(t)]) + \exp(\beta D)\cosh(\beta[E_i + h(t)]) + 1/2} \right\rangle = \langle e^{E_i \nabla} \rangle \left\langle \frac{2\exp(4\beta D)\,\sinh(2\beta[x + h(t)]) + \exp(\beta D)\sinh(\beta[x + h(t)])}{\exp(4\beta D)\,\cosh(2\beta[x + h(t)]) + \exp(\beta D)\cosh(\beta[x + h(t)]) + 1/2} \right\rangle\Big|_{x=0} = \langle e^{E_i \nabla} \rangle f_1[x + h(t)]|_{x=0} \tag{9}$$

and

$$\left\langle \frac{5\sinh\left(\frac{5\beta}{2}[E_j + h(t)]\right) + 3\exp(-4\beta D)\,\sinh\left(\frac{3\beta}{2}[E_j + h(t)]\right) + \exp(-6\beta D)\sinh\left(\frac{\beta}{2}[E_j + h(t)]\right)}{2\cosh\left(\frac{5\beta}{2}[E_j + h(t)]\right) + 2\exp(-4\beta D)\cosh\left(\frac{3\beta}{2}[E_j + h(t)]\right) + 2\exp(-6\beta D)\,\cosh\left(\frac{\beta}{2}[E_j + h(t)]\right)} \right\rangle$$
$$= \langle e^{E_j \nabla} \rangle \left\langle \frac{5\sinh\left(\frac{5\beta}{2}[y + h(t)]\right) + 3\exp(-4\beta D)\,\sinh\left(\frac{3\beta}{2}[y + h(t)]\right) + \exp(-6\beta D)\sinh\left(\frac{\beta}{2}[y + h(t)]\right)}{2\cosh\left(\frac{5\beta}{2}[y + h(t)]\right) + 2\exp(-4\beta D)\cosh\left(\frac{3\beta}{2}[y + h(t)]\right) + 2\exp(-6\beta D)\cosh\left(\frac{\beta}{2}[y + h(t)]\right)} \right\rangle\Big|_{y=0}$$
$$= \langle e^{E_j \nabla} \rangle g_1[y + h(t)]|_{y=0}, \tag{10}$$

where $\nabla = \partial/\partial x$ is a differential operator. Consequently, the expressions of Eqs. (9) and (10) on the magnetizations for a square lattice per A and B sites are obtained as follows:

$$\left\langle \frac{2\exp(4\beta D)\,\sinh(2\beta[E_i + h(t)]) + \exp(\beta D)\sinh(\beta[E_i + h(t)])}{\exp(4\beta D)\,\cosh(2\beta[E_i + h(t)]) + \exp(\beta D)\cosh(\beta[E_i + h(t)]) + 1/2} \right\rangle$$
$$= \langle \sigma_i \rangle = m_A = \left[A(\alpha) + B(\alpha)\langle S_j \rangle + C(\alpha)\langle S_j^2 \rangle + D(\alpha)\langle S_j^3 \rangle + E(\alpha)\langle S_j^4 \rangle + F(\alpha)\langle S_j^5 \rangle\right]^4 f_1(x + h)|_{x=0} \tag{11}$$

and

$$\left\langle \frac{5\sinh\left(\frac{5\beta}{2}[E_j + h(t)]\right) + 3\exp(-4\beta D)\,\sinh\left(\frac{3\beta}{2}[E_j + h(t)]\right) + \exp(-6\beta D)\sinh\left(\frac{\beta}{2}[E_j + h(t)]\right)}{2\cosh\left(\frac{5\beta}{2}[E_j + h(t)]\right) + 2\exp(-4\beta D)\cosh\left(\frac{3\beta}{2}[E_j + h(t)]\right) + 2\exp(-6\beta D)\,\cosh\left(\frac{\beta}{2}[E_j + h(t)]\right)} \right\rangle$$
$$= \langle S_j \rangle = m_B = \left[1 + K(\alpha)\langle \sigma_i \rangle + L(\alpha)\langle \sigma_i^2 \rangle + M(\alpha)\langle \sigma_i^3 \rangle + N(\alpha)\langle \sigma_i^4 \rangle\right]^4 g_1(x + h)|_{x=0}. \tag{12}$$

The Van der Waerden coefficients $A(\alpha)$, $B(\alpha)$, $C(\alpha)$, $D(\alpha)$, $E(\alpha)$, and $F(\alpha)$ for the spin-5/2 in Eq. (11) and $K(\alpha)$, $L(\alpha)$, $M(\alpha)$, and $N(\alpha)$ for the spin-2 in Eq. (12) are given Appendix B. The other order parameters are also given as

follows:

$$\langle\sigma_i^2\rangle = q_A = \left[A(\alpha) + B(\alpha)\langle S_j\rangle + C(\alpha)\langle S_j^2\rangle + D(\alpha)\langle S_j^3\rangle + E(\alpha)\langle S_j^4\rangle + F(\alpha)\langle S_j^5\rangle\right]^4 f_2(x+h)|_{x=0}, \tag{13a}$$

$$\langle\sigma_i^3\rangle = r_A = \left[A(\alpha) + B(\alpha)\langle S_j\rangle + C(\alpha)\langle S_j^2\rangle + D(\alpha)\langle S_j^3\rangle + E(\alpha)\langle S_j^4\rangle + F(\alpha)\langle S_j^5\rangle\right]^4 f_3(x+h)|_{x=0}, \tag{13b}$$

$$\langle\sigma_i^4\rangle = \nu_A = \left[A(\alpha) + B(\alpha)\langle S_j\rangle + C(\alpha)\langle S_j^2\rangle + D(\alpha)\langle S_j^3\rangle + E(\alpha)\langle S_j^4\rangle + F(\alpha)\langle S_j^5\rangle\right]^4 f_4(x+h)|_{x=0}, \tag{13c}$$

and

$$\langle S_j^2\rangle = q_B = \left[1 + K(\alpha)\langle\sigma_i\rangle + L(\alpha)\langle\sigma_i^2\rangle + M(\alpha)\langle\sigma_i^3\rangle + N(\alpha)\langle\sigma_i^4\rangle\right]^4 g_2(x+h)|_{x=0}, \tag{14a}$$

$$\langle S_j^3\rangle = r_B = \left[1 + K(\alpha)\langle\sigma_i\rangle + L(\alpha)\langle\sigma_i^2\rangle + M(\alpha)\langle\sigma_i^3\rangle + N(\alpha)\langle\sigma_i^4\rangle\right]^4 g_3(x+h)|_{x=0}, \tag{14b}$$

$$\langle S_j^4\rangle = \nu_B = \left[1 + K(\alpha)\langle\sigma_i\rangle + L(\alpha)\langle\sigma_i^2\rangle + M(\alpha)\langle\sigma_i^3\rangle + N(\alpha)\langle\sigma_i^4\rangle\right]^4 g_4(x+h)|_{x=0}, \tag{14c}$$

$$\langle S_j^5\rangle = w_B = \left[1 + K(\alpha)\langle\sigma_i\rangle + L(\alpha)\langle\sigma_i^2\rangle + M(\alpha)\langle\sigma_i^3\rangle + N(\alpha)\langle\sigma_i^4\rangle\right]^4 g_5(x+h)|_{x=0}. \tag{14d}$$

The other functions for spin-2, namely, $f_n(x+h)$ $(n = 2, 3, 4)$, and for spin-5/2, namely, $g_k(x+h)(k = 2, 3, 4, 5)$, are defined by

$$f_2(x+h) = \frac{1}{2}\frac{8\,\cosh[2\beta(x+h)] + 2\,\cosh[\beta(x+h)]\exp(-3\beta\,D)}{\cosh[2\beta(x+h)] + \cosh[\beta(x+h)]\exp(-3\beta\,D) + \exp(-4\beta\,D)}, \tag{15a}$$

$$f_3(x+h) = \frac{1}{2}\frac{16\,\sinh[2\beta(x+h)] + 2\,\sinh[\beta(x+h)]\exp(-3\beta\,D)}{\cosh[2\beta(x+h)] + \cosh[\beta(x+h)]\exp(-3\beta\,D) + \exp(-4\beta\,D)}, \tag{15b}$$

$$f_4(x+h) = \frac{1}{2}\frac{32\,\cosh[2\beta(x+h)] + 2\,\cosh[\beta(x+h)]\exp(-3\beta\,D)}{\cosh[2\beta(x+h)] + \cosh[\beta(x+h)]\exp(-3\beta\,D) + \exp(-4\beta\,D)}, \tag{15c}$$

and

$$g_2(y+h) = \frac{25\cosh\left(\frac{5\beta}{2}(y+h)\right) + 9\exp(-4\,\beta D)\cosh\left(\frac{3\beta}{2}(y+h)\right) + \exp(-6\,\beta D)\cosh\left(\frac{\beta}{2}(y+h)\right)}{4\,\cosh\left(\frac{5\beta}{2}(y+h)\right) + 4\exp(-4\,\beta D)\cosh\left(\frac{3\beta}{2}(y+h)\right) + 4\exp(-6\,\beta D)\cosh\left(\frac{\beta}{2}(y+h)\right)}, \tag{16a}$$

$$g_3(y+h) = \frac{125\sinh\left(\frac{5\beta}{2}(y+h)\right) + 27\exp(-4\,\beta D)\cosh\left(\frac{3\beta}{2}(y+h)\right) + \exp(-6\,\beta D)\sinh\left(\frac{\beta}{2}(y+h)\right)}{8\,\cosh\left(\frac{5\beta}{2}(y+h)\right) + 8\exp(-4\,\beta D)\cosh\left(\frac{3\beta}{2}(y+h)\right) + 8\exp(-6\,\beta D)\,\cosh\left(\frac{\beta}{2}(y+h)\right)}, \tag{16b}$$

$$g_4(x+h) = \frac{625\cosh\left(\frac{5\beta}{2}(x+h)\right) + 81\exp(-4\,\beta D)\,\cosh\left(\frac{3\beta}{2}(x+h)\right) + \exp(-6\,\beta D)\cosh\left(\frac{\beta}{2}(x+h)\right)}{16\cosh\left(\frac{5\beta}{2}(x+h)\right) + 16\exp(-4\,\beta D)\cosh\left(\frac{3\beta}{2}(x+h)\right) + 16\exp(-6\,\beta D)\,\cosh\left(\frac{\beta}{2}(x+h)\right)}, \tag{16c}$$

$$g_5(y+h) = \frac{3125\sinh\left(\frac{5\beta}{2}(y+h)\right) + 243\exp(-4\,\beta D)\cosh\left(\frac{3\beta}{2}(y+h)\right) + \exp(-6\,\beta D)\cosh\left(\frac{\beta}{2}(y+h)\right)}{32\,\cosh\left(\frac{5\beta}{2}(y+h)\right) + 32\exp(-4\,\beta D)\cosh\left(\frac{3\beta}{2}(y+h)\right) + 32\exp(-6\,\beta D)\,\cosh\left(\frac{\beta}{2}(y+h)\right)}. \tag{16d}$$

As one can see, in our treatment new order parameters such as q,r, v, and w naturally appear, which one is able to evaluate. This is not the case of the standard MFA, where all correlations are neglected. This is one of the reasons why the present framework provides better results than the standard MFA. We should also mention that the behavior of m, r, and w, as well as q and ν, are similar to each other [32]. Since the model did not include the biquadratic exchange interaction parameter in Eq. (1), we did not investigate the thermal behavior of q and ν.

If we try to treat all the spin-spin correlations exactly for that equation, the problem quickly becomes intractable. A first obvious attempt to deal with it is to ignore the correlations; the decoupling approximation can then be written as

$$\begin{aligned}\langle\sigma_i\,\sigma_{i'}^2\,\ldots\,\sigma_{i^n}^4\rangle &\cong \langle\sigma_i\rangle\langle\sigma_{i'}^2\rangle\ldots\langle\sigma_{i^n}^4\rangle,\\ \langle S_j\,S_{j'}^2\,\ldots\,S_{j^n}^5\rangle &\cong \langle S_j\rangle\langle S_{j'}^2\rangle\ldots\langle S_{j^n}^5\rangle,\end{aligned} \tag{17}$$

with $i \neq i' \neq \cdots \neq i^n$ and $j \neq j' \neq \cdots \neq j^n$ being introduced within the EFT with correlations [29,33,34]. In fact, the approximation corresponds essentially to the Zernike approximation [35] in the bulk problem and has been successfully applied to a great number of magnetic systems including surface problems [29,33], and [34]. On the other hand, in the mean-field theory, all the correlations, including self-correlations, are neglected.

By expanding the right-hand sides of Eqs. (11) and (12) with Eqs. (13) and (14), and applying them to Eqs. (7) and (8), one can obtain the following set of coupled dynamic effective-field equations of motion for the sublattice magnetizations:

$$\begin{aligned}\frac{d}{dt}m_A = &-m_A + a_0 + a_1 m_B + a_2 m_B^2 + a_3 m_B^3 + a_4 m_B^4\\ &+ a_5 m_B^5 + a_6 m_B^6 + a_7 m_B^7 + a_8 m_B^8 + a_9 m_B^9\\ &+ a_{10} m_B^{10} + a_{11} m_B^{11} + a_{12} m_B^{12} + a_{13} m_B^{13} + a_{14} m_B^{14}\\ &+ a_{15} m_B^{15} + a_{16} m_B^{16} + a_{17} m_B^{17} + a_{18} m_B^{18} + a_{19} m_B^{19}\\ &+ a_{20} m_B^{20}\end{aligned} \tag{18}$$

and

$$\frac{d}{dt}m_B = -m_B + b_0 + b_1 m_A + b_2 m_A^2 + b_3 m_A^3 + b_4 m_A^4 + b_5 m_A^5 + b_6 m_A^6 + b_7 m_A^7 + b_8 m_A^8 + b_9 m_A^9 + b_{10} m_A^{10} + b_{11} m_A^{11} + b_{12} m_A^{12} + b_{13} m_A^{13} + b_{14} m_A^{14} + b_{15} m_A^{15} + b_{16} m_A^{16}. \quad (19)$$

The coefficients a_i ($i = 0,1,\ldots,20$) and b_j ($j = 0,1,\ldots,16$) can be easily calculated by employing a mathematical relation $\exp(\alpha\,\nabla)\,f(x) = f(x+\alpha)$. These coefficients are given in Appendix C.

The dynamic order parameters or dynamic magnetizations as the time-averaged magnetization over a period of the oscillating magnetic field are given as

$$M_{A,B} = \frac{w}{2\pi}\oint m_{A,B}(t)\,dt. \quad (20)$$

On the other hand, the hysteresis loop area is

$$A = -\oint m_{A,B}(t)\,dh = -hw\oint m_{A,B}(t)\cos(wt)dt, \quad (21)$$

which corresponds to the energy loss due to the hysteresis. The dynamic correlation is calculated as

$$C = \frac{w}{2\pi}\oint m_{A,B}(t)h(t)dt = \frac{wh}{2\pi}\oint m_{A,B}(t)\sin(wt)dt. \quad (22)$$

We should also mention that the hysteresis loop area A and the dynamic correlation C are also measured in units zJ in the numerical calculations The time variations of the average order parameters, the thermal behavior of the dynamic magnetizations, the hysteresis loop area, and the dynamic correlation will be given and discussed in Sec. III.

III. NUMERICAL RESULTS AND DISCUSSION

A. Time variations of average order parameters

In this section, we study the time variations of the average magnetizations to find the phases in the system. In order to investigate the time variation behaviors of the average magnetizations, first we have to study the stationary solutions of the dynamic effective-field equations, given in Eqs. (18) and (19), when the parameters D/zJ, T/zJ, and h/zJ are varied. The stationary solutions of these equations will be a periodic function of wt with period 2π; that is, $m_A(wt+2\pi) = m_A(wt)$ and $m_B(wt+2\pi) = m_B(wt)$. Moreover, they can be one of two types according to whether they have or do not have the properties

$$m_A(wt+\pi) = -m_A(wt) \quad (23a)$$

and

$$m_B(wt+\pi) = -m_B(wt). \quad (23b)$$

The first type of solution which satisfies both Eqs. (23a) and (23b) is called a symmetric solution and corresponds to a paramagnetic (p) solution. In this solution, the submagnetizations $m_A(wt)$ and $m_B(wt)$ are equal to each other $[m_A(wt) = m_B(wt)]$, and they oscillate around zero and are delayed with respect to the external magnetic field. The second type of solution, which does not satisfy Eqs. (23a) and (23b), is called a nonsymmetric solution, but this solution corresponds to a ferrimagnetic (i) solution because the submagnetizations $m_A(wt)$ and $m_B(wt)$ are not equal to each other $[m_A(wt) \neq m_B(wt)]$, and they oscillate around a nonzero value. Hence, if $m_A(wt)$ and $m_B(wt)$ oscillate around ± 2 and $\pm 5/2$, respectively, this solution is called the ferrimagnetic-I (i_1) phase; if $m_A(wt)$ and $m_B(wt)$ oscillate around ± 1 and $\pm 5/2$, respectively, this solution is called the ferrimagnetic-II (i_2) phase. These facts are seen explicitly by solving Eqs. (18) and (19) numerically. These equations are solved by using the numerical Adams-Moulton predictor-corrector method for a given set of parameters and initial values and are presented in Fig. 1. Figures 1(a) and 1(b) represent the paramagnetic (p) and ferrimagnetic-I (i_1) fundamental phases, respectively, and Figs. 1(c)–1(e) represent the $i_1 + i_2$, $i_1 + p$, and $i_1 + i_2 + p$ mixed phases, respectively.

B. Thermal behavior of the dynamic magnetizations, hysteresis loop area, and correlation

In this section, we investigate the thermal behavior of the average order parameters in a period or the dynamic magnetizations ($M_{A,B}$), hysteresis loop area (A), and correlation (C) as a function of the reduced temperature. We should also mention that in the numerical calculations, the hysteresis loop area A and the dynamic correlation C are also measured in units zJ. In order to investigate the thermal behavior of $M_{A,B}$, A, and C, we solve Eqs. (20), (21), and (22) by combining the numerical methods of the Adams-Moulton predictor corrector with Romberg integration. This study leads us to characterize the nature (continuous or discontinuous) of the dynamic transitions as well as to obtain the DPT points. A few interesting results are plotted in Figs. 2(a)–2(c) in order to illustrate the calculation of the DPT points. In these figures, T_C/zJ and T_t/zJ represent the second- and first-order phase transition temperatures, respectively. Figure 2(a) shows the thermal behavior of $M_{A,B}$, A, and C for $D/zJ = -0.25$ and $h/zJ = 0.15$; $M_A = 2$, and $M_B = 5/2$ at zero temperature, and M_A and M_B decrease to zero continuously as the reduced temperature increases; therefore, a second-order phase transition occurs at $T_C/zJ = 1.625$ and the dynamic phase transition is from the ferrimagnetic-I (i_1) phase to the paramagnetic (p) phase. Moreover, the hysteresis loop area A becomes zero and the dynamic correlation C becomes a minimum negative value at T_C/zJ. In this case, the dynamic nature of the phase transition is independent of the initial values. On the other hand, to see the $i_1 + p$ mixed phase the temperature dependence of $M_{A,B}$, A, and C are plotted for $D/zJ = -0.5$ and $h/zJ = 0.45$ and different initial values, as seen in Figs. 2(b) and 2(c). In Fig. 2(b), $M_A = 2$ and $M_B = 5/2$ at zero temperature and decreases to zero discontinuously as the temperature increases; hence, the system undergoes a first-order phase transition from the i_1 phase to the p phase at $T_t/zJ = 0.55$. Therefore, T_t/zJ is the first-order phase transition temperature where the discontinuity or jump occurs. Moreover, if one increases the reduced temperature from zero, the A and C increase from zero and a certain negative value, respectively, to a certain positive nonzero value, and A suddenly jumps to the lower positive value and C

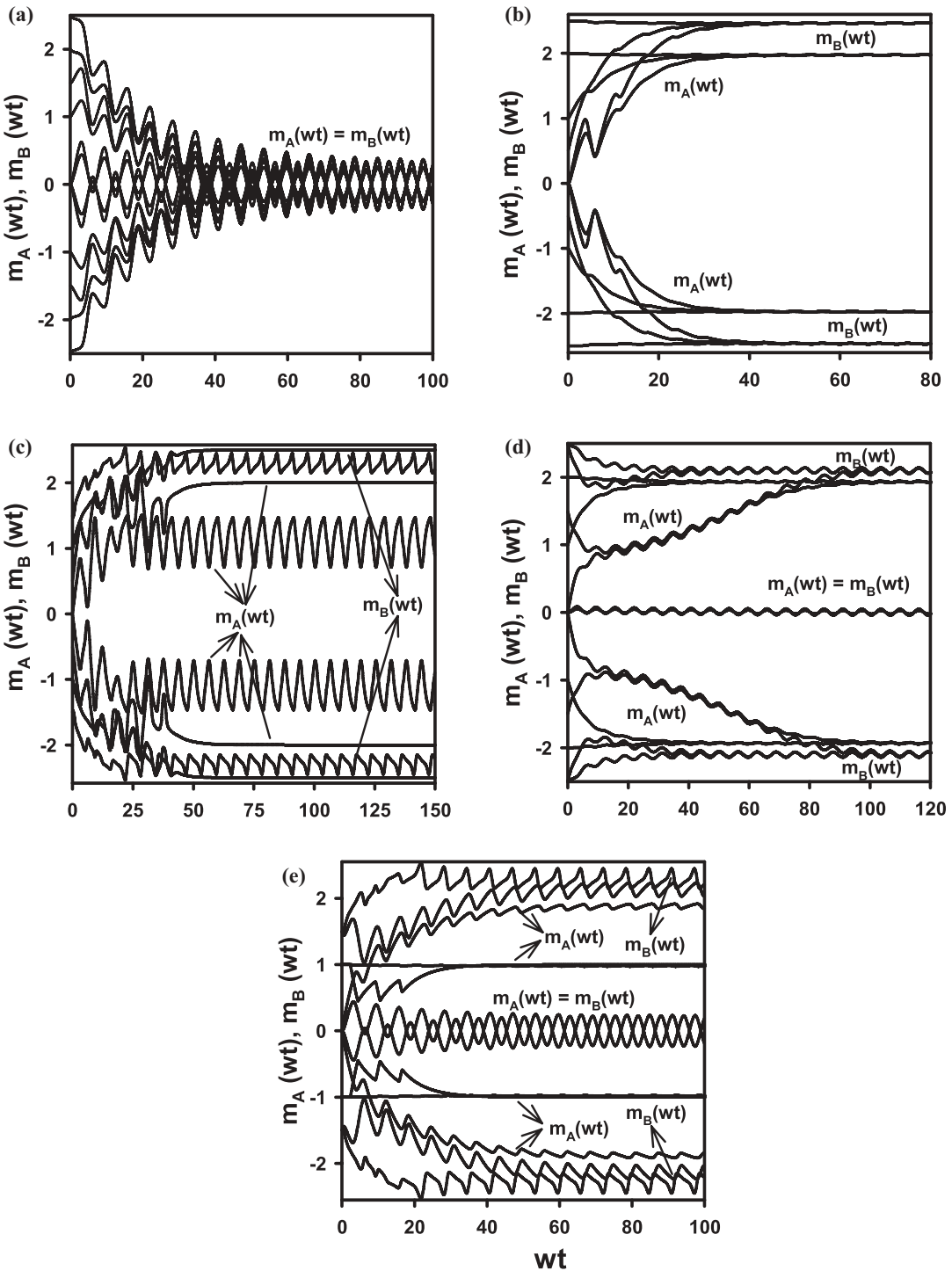

FIG. 1. Time variations of the magnetizations $[m_A(wt), m_B(wt)]$: Exhibiting paramagnetic (p) phase: $D/zJ = 0.025$, $h/zJ = 2.0$, and $T/zJ = 2.0$. (a) Exhibiting ferrimagnetic-I (i_1) phase: $D/zJ = -0.375$, $h/zJ = 1.0$, and $T/zJ = 0.7$. (b) Exhibiting the coexistence region ($i_1 + i_2$): $D/zJ = 0.025$, $h/zJ = 0.5$, and $T/zJ = 1.5$. (c) Exhibiting the coexistence region ($i_1 + p$): $D/zJ = -0.5$, $h/zJ = 1.0$, and $T/zJ = 0.9$. (d) Exhibiting the coexistence region ($i_1 + i_2 + p$): $D/zJ = 0.025$, $h/zJ = 0.5$, and $T/zJ = 1.5$.

jumps to a lower negative value; hence, these behaviors also show that the system undergoes a first-order phase transition at T_t/zJ. Figure 2(c) illustrates that the system does not undergo any phase transitions, but the p phase always exists. Therefore, Figs. 2(b) and 2(c) show that the $i_1 + p$ coexistence region or mixed phase occurs in the system, and this fact is seen in the phase diagram of Fig. 3(e) for $h/zJ = 0.4$, explicitly. For the latter two examples, the dynamic nature of the phase transition strictly depends on the initial values.

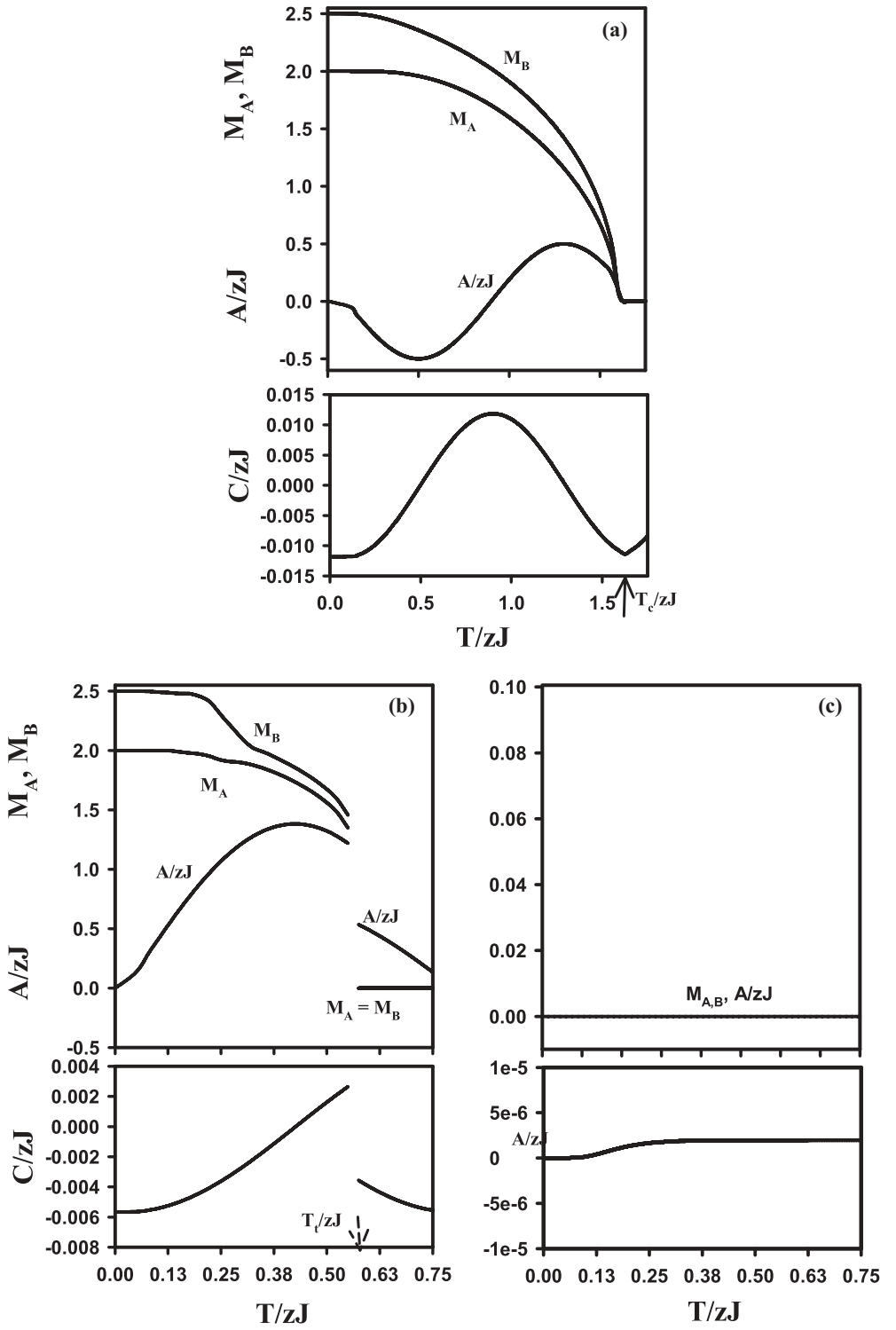

FIG. 2. The reduced temperature dependence of the dynamic magnetizations (M_A and M_B), dynamic hysteresis loop area (A), and dynamic correlation (C) for the various values of D/zJ and h/zJ . T_C/zJ and T_t/zJ are the second- and first-order phase transition temperatures, respectively. (a) Exhibiting a second-order phase transition from the i_1 phase to the p phase for $D/zJ = -0.25$ and $h/zJ = 0.15$; T_C is found at 1.1750. (b) Exhibiting a first-order phase transition from the i_1 phase to the p phase for $D/zJ = -0.5$ and $h/zJ = 0.4$; T_t/zJ is found at 0.55. (c) The system does not undergo any phase transitions, but the p phase always exists for $D/zJ = -0.5$ and $h/zJ = 0.4$.

C. Dynamic phase diagrams

Since we obtained the phases and DPT points in Secs. III A and III B, respectively, we can now present the dynamic phase diagrams of the system. The calculated dynamic phase diagrams in the $(T/zJ, h/zJ)$ plane are presented in Fig. 3 for various values of the interaction parameters. In these phase

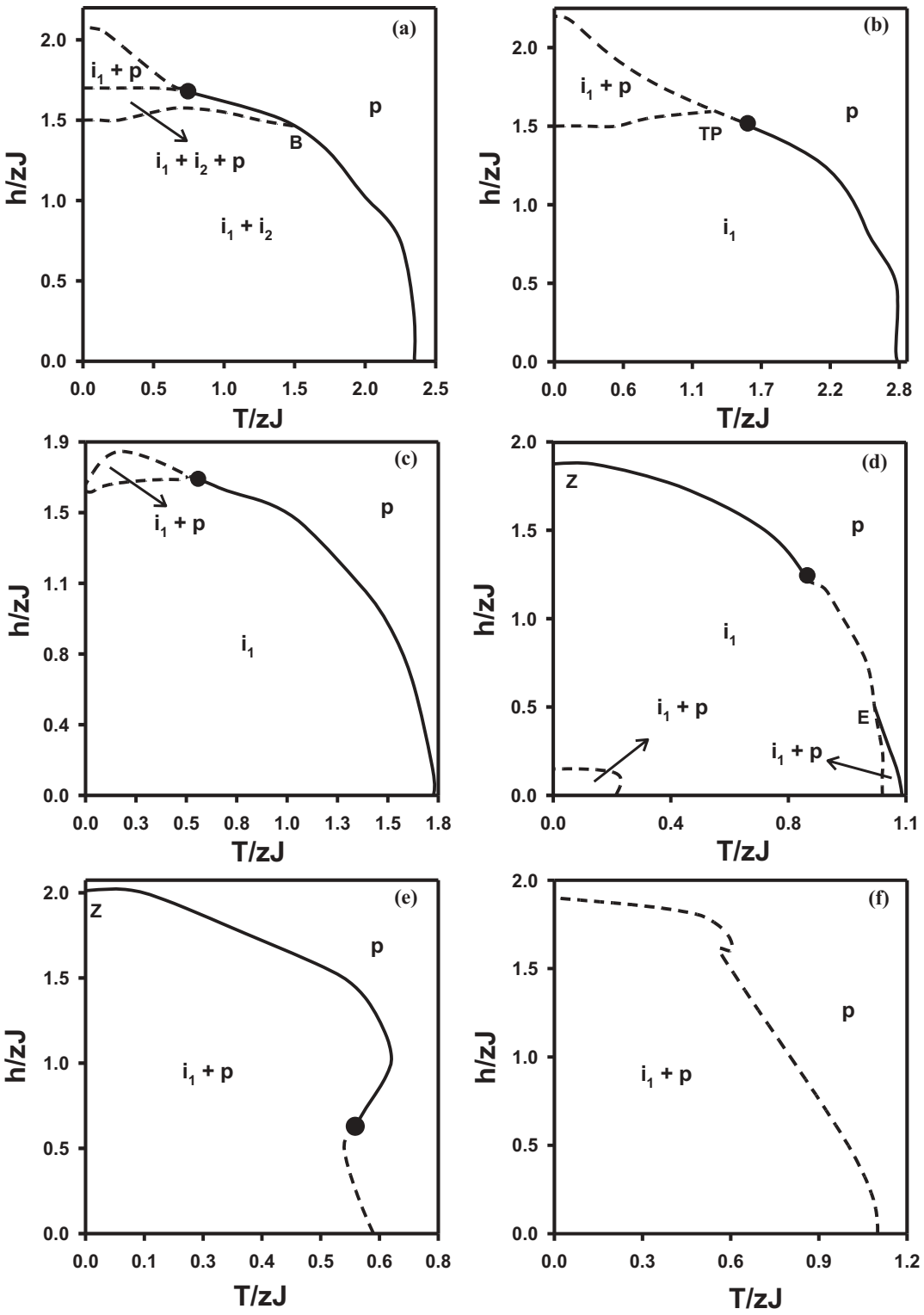

FIG. 3. The dynamic phase diagrams in the $(T/zJ, h/zJ)$ plane. The $i_1 + i_2$, $i_1 + p$, and $i_1 + i_2 + p$ mixed phases in addition to the i_1 and p fundamental phases, depending on the interaction parameter, are found. Dashed and solid lines represent the first- and second-order phase transitions, respectively. The special points are represented as zero-temperature critical (Z), double critical end (B), triple point (TP), and critical end point (E): (a) $D/zJ = 0.025$, (b) $D/zJ = 0.25$, (c) $D/zJ = -0.25$, (d) $D/zJ = -0.375$, (e) $D/zJ = -0.45$, and (f) $D/zJ = -0.5$.

diagrams, the solid and dashed lines represent the second- and first-order phase transition lines, respectively, and the dynamic tricritical point is denoted by a filled circle. B, Z, E, and TP represent the dynamic double critical end point, zero-temperature critical point, triple point, and critical end point, respectively. Moreover, as can be seen in Fig. 4, we

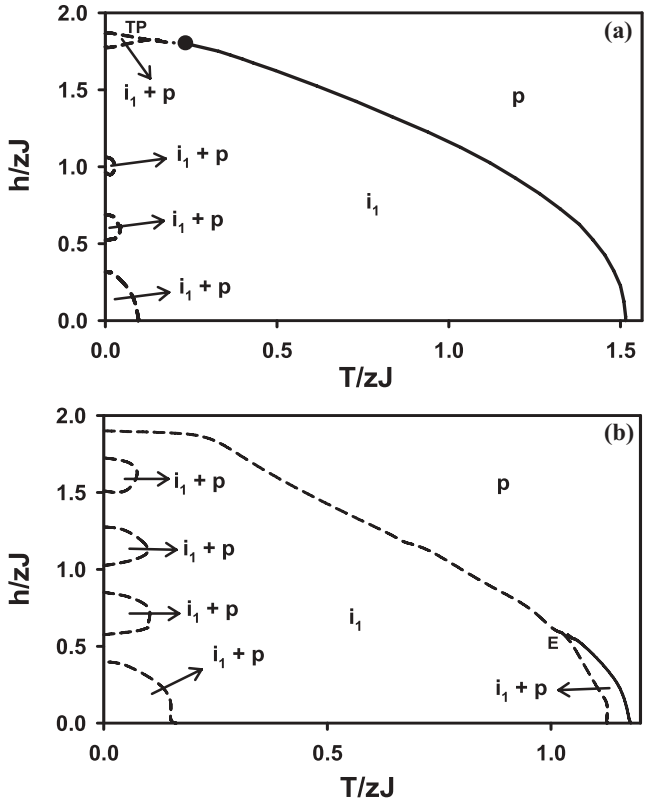

FIG. 4. . Same as Fig. 3, but in the (T/zJ, h/zJ) plane that was obtained for dynamic MFA. The special points are the dynamic tricritical point, which is with a represented filled circle, the dynamic triple point (TP), and the dynamic critical end point (E). (a) $D/zJ = -0.375$, and (b) $D/zJ = -0.45$.

have also presented dynamic phase diagrams in the (T/zJ, h/zJ) plane by using the dynamic MFA in order to see the influence of the correlations and the artifact of some of the first-order transition lines in the dynamic MFA.

For a two-dimensional kinetic mixed Ising system, we plot the dynamic phase diagrams of the system in the ($T/zJ, h/zJ$) plane for various values of D/zJ in Fig. 3 and six main different topological types of phase diagrams are observed. From these phase diagrams the following five interesting phenomena are observed. (1) The phase diagrams in Figs. 3(a)–3(e) illustrate one tricritical point, but Fig. 3(f) does not contain any tricritical point; hence in this figure the dynamic phase line is only a first-order line. (2) In Fig. 3(c), the system also exhibits reentrant behavior, i.e., as the temperature is increased, the system passes from the paramagnetic (p) phase to the i_1 + p coexistence or mixed phase, and back to the p phase again for high values of h/zJ. In spin systems, reentrant behavior can be understood as follows. At high temperatures, the entropy is the most important factor and uncorrelated fluctuations determine the thermodynamics. The system is then in the p phase bias due to the applied field. As the temperature is lowered, the energy and entropy are both important and the correlated fluctuations affect the dominance of either phase significantly. The system enters the ordered phase. At low temperatures, the energy is important, not the entropy, and the system reenters the p phase again [36,37]. (3) Figure 3(a) illustrates a dynamic double critical end point (B), Fig. 3(b) exhibits a triple point (TP), Fig. 3(d) shows both a critical end point (E), and a zero-temperature critical point (Z), and Fig. 3(e) displays only a zero-temperature critical point (Z) besides a tricritical point. We should also mention that a similar phase diagram to Fig. 3(b) was also obtained in kinetic single Ising systems with different spins [5,38,39], except that in those studies the ferrimagnetic phase becomes a ferromagnetic phase and the mixed phase is different. On the other hand, phase diagrams similar to this one have also been obtained in mixed Ising systems [40]. Moreover, a similar phase diagram to Fig. 3(f) has also been obtained in the kinetic spin-2 BC [39], except that the ferrimagnetic phase becomes a ferromagnetic phase. It is worthwhile mentioning that this system does not undergo any dynamic phase transitions for $D/zJ \leqslant -0.5125$, and thus dynamic phase diagrams cannot be obtained for $D/zJ \leqslant -0.5125$ in this system.

We also calculate the phase diagrams and the (T/zJ, h/zJ) plane by using the dynamic MFA, as seen in Fig. 4. Figure 4(a) is calculated for $D/zJ = -0.375$ in the (T/zJ, h/zJ) plane, which corresponds to Fig. 3(d). In this phase diagram, the system exhibits one coexistence region or mixed phase, namely, the i_1 + p mixed phase besides the i_1 and p fundamental phases. Moreover, this system displays a dynamic triple point (TP) besides the dynamic tricritical point. The dynamic phase boundaries among these phases are first-order lines, except for the boundaries between the i_1 and p fundamental phases for high values of T/zJ. For $D/zJ = -0.45$, the phase diagram is presented in Fig. 4(b), which corresponds to Fig. 3(e). The system shows the i_1 + p mixed phase besides the i_1 and p fundamental phases; the system does not contain any tricritical point. Moreover, this system exhibits a critical end point (E). The dynamic phase boundaries among these phases are first-order lines, except for the boundaries between the i_1 + p and p phases for high values of T/zJ.

In order to see the influence of the correlations and artifacts of some of the first-order transition lines in the dynamic MFA, due to its limitations, such as the correlation of spin fluctuations not being considered, we compared Fig. 4(a) with Fig. 3(d) and Fig. 4(b) with Fig. 3(e). From the comparison, the following two fundamental differences were obtained: (i) In Figs. 4(a) and 4(b), the dynamic phase boundaries among the phases are first-order phase transition lines, except for the boundary between the i_1 and p fundamental phases in Fig. 4(a) and the boundary between the i_1 + p and p fundamental phases in Fig. 4(b), which are second-order lines. On the other hand, in Fig. 3(d), the dynamic phase boundaries among the phases are second-order phase transition lines, except for the boundary between the i_1 + p and p phases and that between the i_1 and p fundamental phases, which are first-order lines. In Fig. 3(e), the dynamic phase boundaries among the phases are second-order phase transition lines, except for the boundary between the i_1 + p and p phases for high values of T/zJ and low values of h/zJ, which is a first-order line. Therefore, most of the first-order phase lines either disappear or become second-order lines within the dynamic EFT. (ii) While the dynamic tricritical point occurred within the dynamic MFA for low values of T/zJ and high values of h/zJ, as seen in Fig. 4(a), the phase diagram for the EFT exhibits a dynamic tricritical point for high values of T/zJ and low values of h/zJ

within the dynamic EFT, as seen in Fig. 3(d)). Moreover, the system exhibits a tricritical point in Fig. 3(e), but the system illustrates a dynamic tricritical end point (E) instead of a dynamic tricritical point in Fig. 4(b).

IV. SUMMARY AND CONCLUSION

In this study, we analyzed, within the effective-field theory (EFT) with correlations, the stationary states of the kinetic mixed spin-2 and spin-5/2 Ising ferrimagnetic model Hamiltonian with bilinear (J) and a single-ion potential or crystal-field interaction (D) in the presence of a time-varying (sinusoidal) magnetic field [$h(t) = h_0 \sin(wt)$]. First, we studied the time dependence of the magnetizations for different h/zJ, D/zJ, and T/zJ values in order to find the phases in the system. Then, the dynamic magnetizations, hysteresis loop area, and the dynamic correlation were calculated and investigated as a function of reduced temperature. These studies led us to characterize the nature (first- or second-order) of the dynamic phase transitions as well as to obtain the DPT points. Finally, the dynamic phase diagrams were presented in the (T/zJ, h/zJ) plane. We found that the behavior of the system strongly depends on the values of the interaction parameter and six fundamental phase diagrams were obtained in the (T/zJ, h/zJ) plane. The phase diagrams exhibited the i_1, i_2, and p fundamental phases and three mixed phases composed of binary and ternary combinations of the fundamental phases, depending on the interaction parameters. We also compared the results with the results of the dynamic MFA calculation and found that some of the first-order lines and dynamic tricritical points did not appear within the dynamic EFT; they only existed within the framework of the dynamic MFA. Therefore, one concludes that these first-order lines as well as dynamic tricritical points are the artifact of the dynamic MFA calculation.

Finally, we hope this study will contribute to the theoretical and experimental research on the dynamic magnetic properties of kinetic mixed Ising systems as well as to research on magnetism. We also hope that this work will stimulate theoretical physicists to continue to obtain more theoretical results about the dynamic properties of mixed Ising systems by using more accurate techniques such as dynamic Monte Carlo (MC) simulations. Moreover, we hope our results will be helpful in the time-consuming process of determining critical behavior while using dynamic MC simulations.

ACKNOWLEDGMENTS

This work was supported by Erciyes University Research Funds, Grant No: FBD-10-3047. M.E. would like to express his gratitude to TÜBİTAK for support through a scholarship.

APPENDIX A: THE VALUES OF $W_i^A(\sigma_i \to \sigma_i')$

The probabilities $W_i^A(\sigma_i \to \sigma_i')$ in Eq. (6) are calculated as follows:

$$
\begin{aligned}
W_i^A(2\to 0) &= W_i^A(1\to 0) = W_i^A(-1\to 0) = W_i^A(-2\to 0) = W_i^A(0)\\
&= \frac{1}{\tau}\frac{1}{2\exp(\beta D)\cosh(\beta x) + 2\exp(4\beta D)\cosh(2\beta x) + 1},\\
W_i^A(2\to 1) &= W_i^A(0\to 1) = W_i^A(-1\to 1) = W_i^A(-2\to 1) = W_i^A(1)\\
&= \frac{1}{\tau}\frac{\exp(\beta x)\exp(\beta y)}{2\exp(\beta D)\cosh(\beta x) + 2\exp(4\beta D)\cosh(2\beta x) + 1},\\
W_i^A(1\to 2) &= W_i^A(0\to 2) = W_i^A(-1\to 2) = W_i^A(-2\to 2) = W_i^A(2)\\
&= \frac{1}{\tau}\frac{\exp(2\beta x)\exp(4\beta D)}{2\exp(\beta D)\cosh(\beta x) + 2\exp(4\beta D)\cosh(2\beta x) + 1},\\
W_i^A(2\to -1) &= W_i^A(1\to -1) = W_i^A(0\to -1) = W_i^A(-2\to -1) = W_i^A(-1)\\
&= \frac{1}{\tau}\frac{\exp(-\beta x)\exp(\beta D)}{2\exp(\beta D)\cosh(\beta x) + 2\exp(4\beta D)\cosh(2\beta x) + 1},\\
W_i^A(2\to -2) &= W_i^A(1\to -2) = W_i^A(0\to -2) = W_i^A(-1\to -2) = W_i^A(-2)\\
&= \frac{1}{\tau}\frac{\exp(-2\beta x)\exp(4\beta D)}{2\exp(\beta D)\cosh(\beta x) + 2\exp(4\beta D)\cosh(2\beta x) + 1},
\end{aligned}
$$

where $x = J\sum_j S_j^B + h(t)$.

APPENDIX B: THE VAN DER WAERDEN COEFFICIENTS

The Van der Waerden coefficients $A(\alpha)$, $B(\alpha)$, $C(\alpha)$, $D(\alpha)$, $E(\alpha)$, and $F(\alpha)$ for the spin-5/2 in Eq. (11), and $K(\alpha)$, $L(\alpha)$, $M(\alpha)$, and $N(\alpha)$ for the spin-2 in Eq. (12) are given as follows:

$$
\begin{aligned}
A(\alpha) &= \frac{1}{128}\left[3\cosh\left(\frac{5\alpha}{2}\right) - 25\cosh\left(\frac{3\alpha}{2}\right) + 150\cosh\left(\frac{\alpha}{2}\right)\right],\\
B(\alpha) &= \frac{1}{960}\left[9\sinh\left(\frac{5\alpha}{2}\right) - 125\sinh\left(\frac{3\alpha}{2}\right) + 2250\sinh\left(\frac{\alpha}{2}\right)\right],
\end{aligned}
$$

$$C(\alpha) = \frac{1}{48}\left[-5\cosh\left(\frac{5\alpha}{2}\right) + 39\cosh\left(\frac{3\alpha}{2}\right) - 34\cosh\left(\frac{\alpha}{2}\right)\right],$$
$$D(\alpha) = \frac{1}{24}\left[-\sinh\left(\frac{5\alpha}{2}\right) + 13\sinh\left(\frac{3\alpha}{2}\right) - 34\sinh\left(\frac{\alpha}{2}\right)\right],$$
$$E(\alpha) = \frac{1}{24}\left[\cosh\left(\frac{5\alpha}{2}\right) - 3\cosh\left(\frac{3\alpha}{2}\right) + 2\cosh\left(\frac{\alpha}{2}\right)\right],$$
$$F(\alpha) = \frac{1}{60}\left[\sinh\left(\frac{5\alpha}{2}\right) - 5\sinh\left(\frac{3\alpha}{2}\right) + 10\sinh\left(\frac{\alpha}{2}\right)\right],$$

and

$$K(\alpha) = \tfrac{1}{6}[8\sinh(\alpha) - \sinh(2\alpha)], \quad L(\alpha) = \tfrac{1}{12}[16\cosh(\alpha) - \cosh(2\alpha) - 15],$$
$$M(\alpha) = \tfrac{1}{6}[\sinh(2\alpha) - 2\sinh(\alpha)], \quad N(\alpha) = \tfrac{1}{12}[\cosh(2\alpha) - 4\cosh(\alpha) + 3],$$

where $\alpha = J\nabla$.

APPENDIX C: THE COEFFICIENTS a_i AND b_j

The coefficients a_i ($i = 0, 1, \ldots, 20$) and b_j ($j = 0, 1, \ldots, 16$) in Eqs. (18) and (19) are defined as follows:

$$a_0 = \frac{1}{4294967296}\begin{bmatrix} 81\,f_1(h-10J) - 2700\,f_1(h-9J) + 49950\,f_1(h-8J) - 576300\,f_1(h-7J) \\ +4572925\,f_1(h-6J) - 23752176\,f_1(h-5J) + 75239400\,f_1(h-4J) \\ -59476400\,f_1(h-3J) - 342915150\,f_1(h-2J) + 1157549400\,f_1(h-J) \\ +2673589236\,f_1(0) + 1157549400\,f_1(h+J) - 342915150\,f_1(h+2J) \\ -59476400\,f_1(h+3J) + 75239400\,g(h+4J) - 23752176\,g(h+5J) \\ +4572925\,f_1(h+6J) - 576300\,f_1(h+7J) + 49950\,f_1(h+8J) - 2700\,f_1(h+9J) \\ +81\,f_1(h+10J) \end{bmatrix},$$

$$a_1 = \frac{1}{8053063680}\begin{bmatrix} -243\,f_1(h-10J) + 9450\,f_1(h-9J) - 232200\,f_1(h-8J) + 3500550\,f_1(h-7J) \\ -36915425\,f_1(h-6J)260628264\,f_1(h-5J) - 1238698800\,f_1(h-4J) \\ +3102663800\,f_1(h-3J) - 1437457950\,f_1(h-2J) - 18688785300\,f_1(h-J) \\ +18688785300\,f_1(h+J) + 1437457950\,f_1(h+2J) - 3102663800\,f_1(h+3J) \\ +1238698800\,f_1(h+4J) - 260628264\,f_1(h+5J) + 36915425\,f_1(h+6J) \\ -3500550\,f_1(h+7J) + 232200\,f_1(h+8J) - 9450\,f_1(h+9J) + 243\,f_1(h+10J) \end{bmatrix},$$

$$\vdots$$

$$a_{20} = \frac{1}{207360000}\begin{bmatrix} f_1(h-10J) - 20\,f_1(h-9J) + 190\,f_1(h-8J) - 1140\,f_1(h-7J) + 4845\,f_1(h-6J) \\ -15504\,f_1(h-5J) + 38760\,f_1(h-4J) - 77520\,f_1(h-3J) + 125970\,f_1(h-2J) \\ -167960\,f_1(h-J) + 184756\,f_1(h) - 167960\,f_1(h+J) + 125970\,f_1(h+2J) \\ -77520\,f_1(h+3J) + 38760\,f_1(h+4J) - 15504\,f_1(h+5J) + 4845\,f_1(h+6J) \\ -1140\,f_1(h+7J) + 190\,f_1(h+8J) - 20\,f_1(h+9J) + f_1(h+10J) \end{bmatrix},$$

$$b_0 = g_1(h),$$
$$b_1 = -\tfrac{1}{3}[-g_1(h-2J) + 8g_1(h-J) - 8g_1(h+J) + g_1(h+2J)],$$
$$\vdots$$

$$b_{16} = -\frac{1}{331776}\begin{bmatrix} -12870g_1(h) - g_1(h-8J) - 16g_1(h-7J) + 120g_1(h-6J) - 560g_1(h-5J) + 1820g_1(h-4J) \\ -4368g_1(h-3J) + 8008g_1(h-2J) - 11440g_1(h-J) + 8008g_1(h+2J) - 4368g_1(h+3J) \\ +1820g_1(h+4J) - 560g_1(h+5J) + 120g_1(h+6J) - 16g_1(h+7J) + g_1(h+8J) \end{bmatrix}.$$

[1] See, e.g., H. E. Stanley, *Introduction to the Phase Transitions and Critical Phenomena* (Oxford University Press, Qxford, 1971); S. K. Ma, *Modern Theory of Critical Phenomena* (W. A. Benjamin, Inc., Reading, MA, 1976).

[2] B. K. Chakrabarti and M. Acharyya, Rev. Mod. Phys. **71**, 847 (1999); G. Korniss, P. A. Rikvold and M. A. Novotny, Phys. Rev. E **66**, 056127 (2002); T. Yasui, H. Tutu, M. Yamamoto and H. Fujisaka, *ibid.* **66**, 036123 (2002); H. Tutu and N. Fujiwara, J. Phys. Soc. Jpn. **73**, 2680 (2004); M. Acharyya, Int. J. Mod. Phys. C **16**, 1631 (2005); M. Keskin, O. Canko, and U. Temizer, Phys. Rev. E **72**, 036125 (2005); Th. Braun, W. Kleemann, J. Dec, and P. A. Thomas, Phys. Rev. Lett. **94**, 117601 (2005); E. Machado, G. M. Buendía, P. A. Rikvold, and R. M. Ziff, Phys. Rev. E **71**, 016120 (2005); O. Canko, Ü. Temizer, and

M. Keskin, Int. J. Mod. Phys. C **17**, 1717 (2006); M. Keskin, O. Canko, and B. Deviren, Phys. Rev. E **74**, 011110 (2006); T. Vojta and M. Y. Lee, Phys. Rev. Lett. **96**, 035701 (2006); N. Fujiwara, T. Kobayashi, and H. Fuhisaka, Phys. Rev. E **75**, 026202 (2007); G. Berkolaiko and M. Grinfeld, *ibid.* **76**, 061110 (2007); T. Ma and S. Wang, J. Math. Phys. **49**, 053506 (2008); S. A. Deviren and E. Albayrak, Phys. Rev. E **82**, 022104 (2010).

[3] M. Keskin and M. Ertaş, Phys. Rev. E **80**, 061140 (2009).

[4] X. L. Shi, G. Z. Wei, and L. Li, Phys. Lett. A **372**, 5922 (2008); B. Deviren, O. Canko, and M. Keskin, Chin. Phys. B **19**, 050518 (2010); X. L. Shi and G. Z. Wei, Phys. Lett. A **374**, 1885 (2010).

[5] Y. Yüksel, E. Vatansever, Ü. Akinci, and H. Polat, Phys. Rev. E **85**, 051123 (2012); B. Deviren and M. Keskin, Phys. Lett. A **376**, 1011 (2012).

[6] E. Costabile and J. R. de Sousa, Phys. Rev. E **85**, 011121 (2012).

[7] X. Shi and G. Wei, Physica A **391**, 29 (2012); B. Deviren and M. Keskin, J. Magn. Magn. Mater. **324**, 1051 (2012).

[8] G. Gulpinar and E. Vatansever, J. Stat. Phys. **146**, 787 (2012); E. Castabile, O. R. Salmon, and J. R. de Sousa, Eur. Phys. J. B **85**, 123 (2012).

[9] Q. Jiang, H. N. Yang, and G. C. Wang, Phys. Rev. B **52**, 14911 (1995).

[10] Z. A. Samoilenko, V. D. Okunev, E. I. Pushenko, V. A. Isaev, P. Gierlowski, K. Kolwas, and S. J. Lewandowski, Inorg. Mater. **39**, 836 (2003).

[11] W. Kleemann, T. Braun, J. Dec, and O. Petracic, Phase Transitions **78**, 811 (2005).

[12] D. T. Robb, Y. H. Xu, O. Hellwig, J. McCord, A. Berger, M. A. Novotny, and P. A. Rikvold, Phys. Rev. B **78**, 134422 (2008).

[13] K. Kanuga and M. Çakmak, Polymer **48**, 7176 (2007).

[14] N. Gedik, D. S. Yang, G. Logvenov, I. Bozovic, and A. H. Zewail, Science **20**, 425 (2007).

[15] M. Monsuripur, J. Appl. Phys. **61**, 1580 (1987).

[16] *From Molecular Assemblies to the Devices*, edited by O. Kahn and E. Coronado *et al.* (Kluwer Academic Publishers, Dordrecht, 1996).

[17] T. Kaneyoshi, Y. Nakamura, and S. Shin, J. Phys.: Condens. Matter **10**, 7025 (1999).

[18] Y. Yakamura, S. Shin, and T. Kaneyoshi, Physica B **284-288**, 1479 (2000).

[19] Y. Nakamura, Prog. Theor. Phys. Suppl. **138**, 466 (2000); Phys. Rev. B **62**, 11742 (2000).

[20] J. Li, A. Du, and G. Wei, Physica B **348**, 79 (2004).

[21] W. Jiang, C. Liu, and Y. Jiang, Physica A **389**, 2227 (2010).

[22] H. K. Mohammad, E. P. Domashhevskaya, and A. F. Klinskikh, Solid State Commun. **150**, 1253 (2010).

[23] N. De La Espriella and G. M. Buendía, J. Phys.: Condens. Matter **23**, 176003 (2011).

[24] E. Albayrak, Phys. Lett. A **372**, 361 (2008).

[25] A. A. Bukharov, A. S. Ovhinnikov, N. V. Baranopv, and K. Inoune, Eur. Phys. J. B **70**, 369 (2009).

[26] M. Ertaş, M. Keskin, and B. Deviren, J. Stat. Phys. **140**, 934 (2012).

[27] M. Ertaş, M. Keskin, and B. Deviren, Physica A **391**, 1038 (2012).

[28] R. J. Glauber, J. Math. Phys. **4**, 294 (1963).

[29] R. Honmura and T. Kaneyoshi, J. Phys. C: Solid State Phys. **12**, 3979 (1979).

[30] T. Kaneyoshi, I. P. Fittipaldi, R. Honmura, and T. Manabe, Phys. Rev. B **24**, 481 (1981).

[31] H. B. Callen, Phys. Lett. **4**, 161 (1963).

[32] T. Kaneyoshi and A. Benyoussef, Phys. Status Solidi B **178**, 233 (1993).

[33] T. Kaneyoshi and H. Beyer, J. Phys. Soc. Jpn. **49**, 1306 (1980).

[34] T. Kaneyoshi, R. Honmura, I. Tamura, and E. F. Sarmento, Phys. Rev. B **29**, 5121 (1984); T. Kaneyoshi, *ibid.* **33**, 7688 (1986).

[35] F. Zernike, Physica **7**, 565 (1940).

[36] M. Keskin, M. A. Pınar, A. Erdinç, and O. Canko, Physica A **364**, 263 (2006).

[37] K. Hui, Phys. Rev. B **38**, 802 (1988).

[38] M. Keskin, O. Canko, and E. Kantar, Int. J. Mod. Phys. C **17**, 1239 (2006); M. Keskin and M. Ertaş, Phase Transitions **83**, 349 (2010); S. A. Deviren and E. Albayrak, Physica A **390**, 3283 (2011); M. Ertaş, M. Keskin, and B. Deviren, J. Magn. Magn. Mater. **324**, 1503 (2012).

[39] M. Ertaş, B. Deviren, and M. Keskin, J. Magn. Magn. Mater. **324**, 704 (2012).

[40] G. M. Buendía and E. Machado, Phys. Rev. E **58**, 1260 (1998); M. Godoy and W. Figueiredo, *ibid.* **66**, 036131 (2002); M. Keskin, O. Canko, and E. Kantar, *ibid.* **77**, 051130 (2008).